Gigagauss magnetic field generation by bladed microtube implosion

M. Murakami

Institute of Laser Engineering, The University of Osaka

I. INTRODUCTION

Ultrahigh magnetic fields play a crucial role in high-energy-density (HED) physics and laboratory astrophysics, enabling the study of extreme astrophysical phenomena[1,2], enhancing plasma confinement in fusion applications[3,4], and facilitating high-energy particle acceleration and radiation generation[5–7].

Among them, the microtube implosion (MTI) scheme, illustrated in Fig. 1, has demonstrated the ability to produce megatesla-level magnetic fields[8]. In this scheme, a hollow cylindrical target with inner radius $R_0 \sim 1$–10 μm is irradiated by ultra-intense femtosecond laser pulses ($I_L \sim 10^{20}$–10^{22} W/cm^2), producing hot electrons of MeV energies. These hot electrons form a sheath field along the inner wall, which accelerates ions radially inward (implosion). A seed magnetic field deflects the ions and electrons in opposite azimuthal directions via the Lorentz force, inducing loop currents ($J_{i\phi}$ and $J_{e\phi}$) in the same direction, ultimately generating a strong axial magnetic field B_c. While effective, this scheme requires a kT-level seed field, introducing system complexity and limiting compact implementation.

To overcome these limitations, we propose a new concept: the bladed microtube implosion (BMI), illustrated in Fig. 2. The BMI scheme employs a hollow cylindrical target with a periodically slanted inner surface resembling sawtooth-shaped blades. This design breaks the cylindrical symmetry of the imploding plasma, causing azimuthally asymmetric ion acceleration and generating a spontaneous loop current around the center[9]. This self-generated current gives rise to a gigagauss-level axial magnetic field, even in the absence of an externally applied seed field.

The acceleration mechanism underlying BMI is conceptually akin to target normal sheath acceleration (TNSA), where laser-driven hot electrons rapidly escape into the central vacuum, creating sheath fields that accelerate ions normal to the inner surface. In BMI, the blade geometry redirects these ions slightly off-axis, inducing a net loop current that seeds the magnetic field. This geometry-driven anisotropy enables spontaneous field generation through collective plasma dynamics.

Unlike conventional flux compression schemes[10–12] that rely on compressing an initially applied seed magnetic field, the present bladed microtube implosion (BMI) concept fundamentally differs in its mechanism. Here, no external magnetic field is required at the outset. Instead, a spontaneous loop current is self-consistently generated near the center due to the asymmetric ion acceleration induced by the blade geometry. This loop current acts as an intrinsic seed, which is then amplified through collective plasma motion during the implosion process. The resulting magnetic field emerges from zero and grows rapidly to gigagauss levels, marking a distinct paradigm shift from seed-field compression to geometry-driven magnetic field creation.

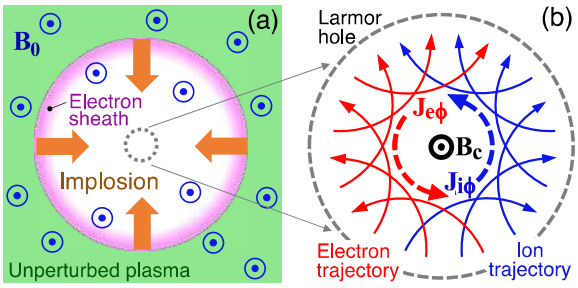

FIG. 1. (a) Top view of inner plasma dynamics during microtube implosion. Isothermal expansion of the inner-wall plasma into vacuum is driven by laser-produced hot electrons. (b) An ultrahigh magnetic field B_c forms at the center, induced by collective currents of ions and electrons deflected in opposite directions by the seed field B_0. Reproduced from Ref.[8].

II. PIC SIMULATIONS OF BLADED MICROTUBE IMPLOSION

A. Setup and laser configuration

The blade structure is intended to provide non-uniform initial conditions for the ion and electron flow under laser irradiation by geometrically breaking the symmetry, thus facilitating the spontaneous generation and amplification of the azimuthal electric current and magnetic

field. Below we perform 2D PIC simulations of BMI using the fully relativistic open-source code EPOCH[13]. The simulation box placed on the x–y plane has a size of 22μm×22μm at a rate of 100 cells/μm or equivalently 10 nm/cell. The system is assumed to be uniform along the z-axis. Carbon with an initial density of $n_{i0} = 3 \times 10^{22}\text{cm}^{-3}$ is employed as the target material in this study, which is assumed to be fully ionized at the ionizatin state $Z = 6$, and the corresponding initial electron density is therefore $n_{e0} = 1.8 \times 10^{23}\text{cm}^{-3}$. Each square cell for the target material is filled with 100 pseudo ions and 200 pseudo electrons.

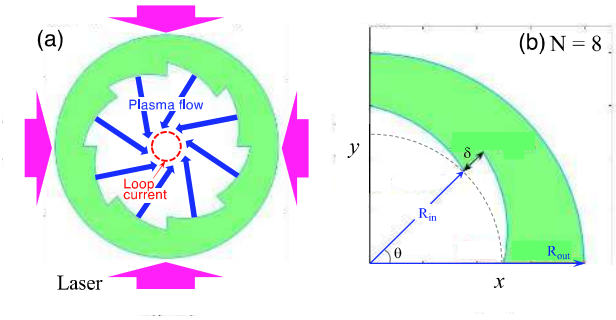

FIG. 2. (a) Core mechanism of BMI: blade heating by hot electrons drives azimuthal ion motion, inducing a loop current and ultrahigh magnetic field. (b) Example with eight blades.

In our simulations, both ions and electrons are treated as fully kinetic particles using the standard particle-in-cell (PIC) method implemented in the EPOCH code. In the simulations, a realistic proton-to-electron mass ratio $m_p/m_e = 1836$ is employed (the mass of a carbon ion is $m_i = 12m_p$). Binary collisions and ionization processes are neglected in this study, since the plasma is considered collisionless over the short laser interaction timescale (~ 100 fs). These approximations are justified by the relativistic energies of the electrons and the extremely high temperature of the system, where collective electromagnetic effects dominate the particle dynamics.

The target structure of BMI is characterized by four free parameters, i.e., the number of blades N, the innermost radius R_{in}, the outer radius R_{out}, and the gap on the blade edge δ. In Fig. 2b, $N = 8$, $R_{\text{in}} = 5\,\mu$m, $R_{\text{out}} = 8\,\mu$m, and $\delta = 1\,\mu$m are employed as an example set of the parameters. The elementary shape of the bladed inner surface is given by a sinusoidal curve in this study, i.e., $r(\theta) = R_{\text{in}} + \delta \sin(N\theta/4)$ for $0 \le \theta \le 2\pi/N$, which is periodically assigned along the inner circle ($0 \le \theta \le 2\pi$) to form N-blades.

Four linear-polarized laser pulses with laser wavelength of $\lambda_L = 0.8\mu$m and the peak intensity $I_L \sim 10^{21}$ W/cm^2 propagate toward the BMI target located at the center along the $\pm x$- and $\pm y$-axes. The polarization of the incident laser pulses are specified such that the electric field and the magnetic field components oscillate on the x-y plane and along z-axis, respectively. The temporal profiles of the incident laser pulses have Gaussian distribution with the pulse duration $\tau_L = 100$ fs (FWHM: full width at half maximum), while the transverse profiles of the pulses are assumed to be plane waves.

B. Implosion dynamics

Figures 3(a)–(d) and 3(e)–(h) depict the temporal evolution of ion and electron density distributions, respectively, at four representative time points: $t = 125$, 240, 300, and 600 fs. These snapshots reveal the dynamic progression of the system throughout the implosion process. Upon irradiation by intense laser pulses, hot electrons generated at the outer surface rapidly traverse to the inner surface of the microtube and penetrate into the central vacuum region of the hollow target. This inward electron flux forms a sheath that induces a quasistatic electric field near the inner wall, which in turn accelerates wall ions toward the central axis [Figs. 3(a), 3(b), 3(e), and 3(f)]. Notably, as seen in Fig. 3(b), the resulting ion flow exhibits a symmetric off-center pattern, consistent with expectations based on the target geometry. As the imploding plasma front, composed of both ions and electrons, passes near the center of the target, a characteristic ring structure—referred to as a "Larmor hole"—emerges around the central region [Figs. 3(c) and 3(g)]. The Larmor hole typically measures 1–2 μm in diameter and represents the envelope of the gyro-orbits of charged particles. In a conventional microtube target without any inner-wall blade structure, the Larmor hole forms due to the deflection of particles by seed magnetic fields on the order of kilotesla.[8] In contrast, in the BMI target, it arises from the geometrical asymmetry introduced by the blades, which induce a pronounced vortex-like motion of ions and electrons during the implosion.

Figures 3(i)–(l) and 3(m)–(p) show the temporal evolution of the ion and electron velocity fields and the magnetic field distributions, respectively. At the peak time of the magnetic field, as illustrated in Fig. 3(k), vortex motions of the ions and electrons are clearly observed—anticlockwise for ions and clockwise for electrons. This converging vortex configuration, consisting of clockwise electron motion and counterclockwise ion motion, forms a quasi-stationary current loop centered near the axis. This self-organized flow pattern underlies the magnetized stagnation structure clearly observed in Fig. 3(o). These counter-rotating flows act cooperatively to generate a strong azimuthal loop current on the order of peta-amperes per square centimeter in the anticlockwise direction. This intense current gives rise to a localized magnetic field of approximately 500 kT at the center, confined within an ellipsoidal region with major and minor axes of 2 μm and 1 μm, respectively, as seen in Fig. 3(o). It is worth noting that the formation of such vortex structures and the associated magnetic field

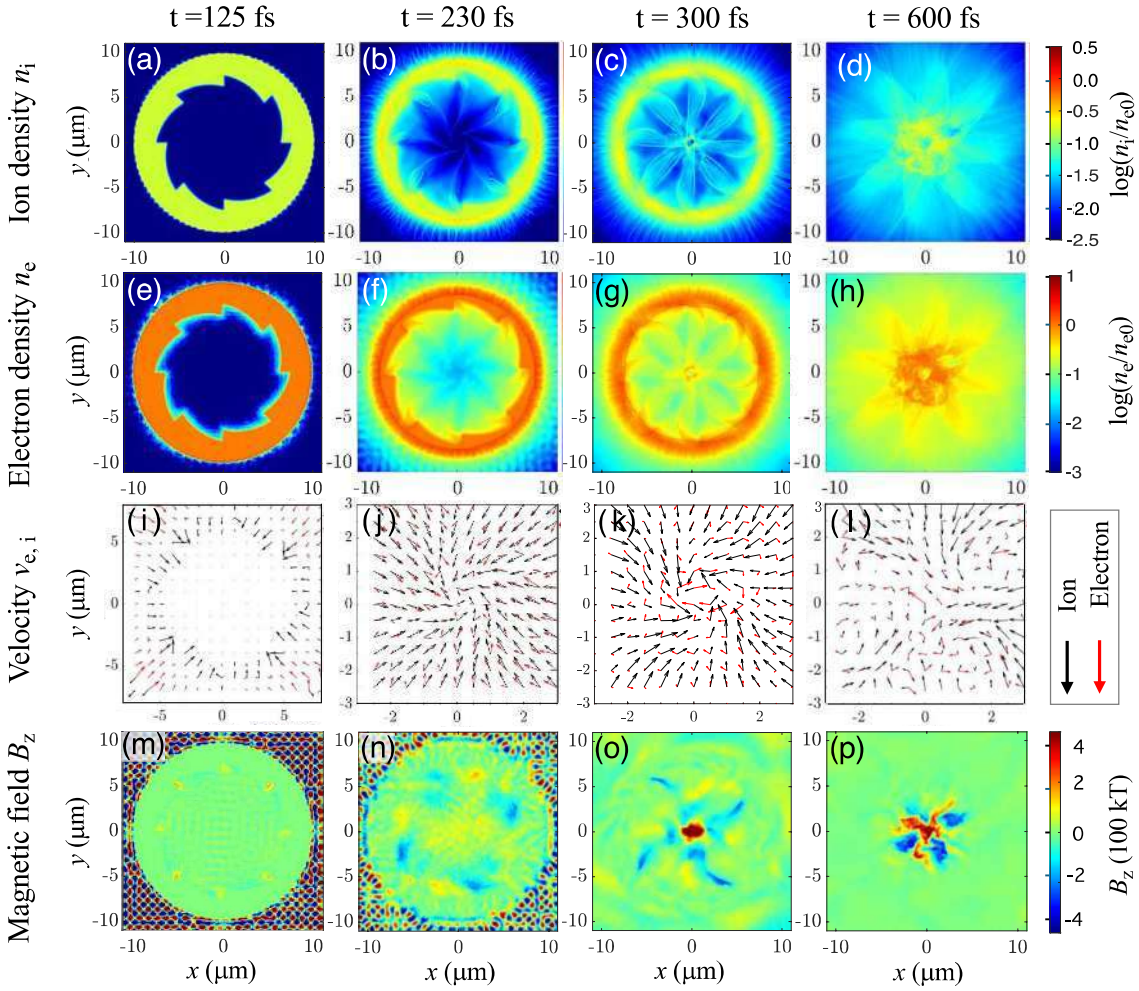

FIG. 3. Two-dimensional distributions of key physical quantities at four different times, under a laser pulse duration of $\tau_L = 100$ fs and peak time $t_p = 150$ fs. (a)–(d): ion density n_i; (e)–(h): electron density n_e; (i)–(l): Velocities of ions (black arrows) and electrons (red arrows), showing anticlockwise ion motion and clockwise electron motion in the central region, resulting in the same anticlockwise current generation. This converging vortex pattern forms the core of the stagnation structure.; (m)–(p): axial magnetic field B_c.

arises through a self-consistent positive feedback mechanism. Specifically, the initial loop current amplifies the central magnetic field, which in turn constrains the motion of charged particles more tightly via the Lorentz force—thereby reinforcing and further intensifying the loop current itself.

C. Magnetic field formation

Figure 4 shows the energy spectra of ions and electrons at two different times before ($t = 200$ fs) and after ($t = 300$ fs) the collapse of converging plasma at the center. The electron energy spectra at the both times are found to be well fitted by the Maxwell distribution with a temperature of $T_e \simeq 13$ MeV (compare the fitted curve). This electron temperature can be well explained by the ponderomotive scaling[14], i.e., $T_e(\mathrm{MeV}) \approx 14\sqrt{I_{L21}\lambda_{L\mu m}^2}$, where I_{L21} and $\lambda_{L\mu m}$ are the laser intensity and the laser wavelength in units of 10^{21} W/cm^2 and μm, respectively. The scaling reads $T_e \sim 11$ MeV by applying $I_L = 10^{21}$ W/cm^2 and $\lambda_L = 0.8\mu$m. Besides, the high energy tail of the ion distribution is also found to have a similar temperature, $T_i \simeq 13$ MeV. While the ion temperature and the electron temperature are kept close to each other in the implosion phase ($t = 200$ fs), i.e., $T_e \approx T_i$, the kinetic energy of an imploding ion increases in time due to adiabatic expansion. The implosion velocity v_{imp} is then roughly estimated to reach the order of the sound speed, i.e., $v_{imp} \sim (1-2)c_s \sim (2.5-5.0) \times 10^9$ cm/s,

where the sound speed $c_s = \sqrt{ZT_e/m_i}$ is calculated with the aid of $T_e = 13$ MeV. The estimates well explain the obtained simulation result, $v_{\rm imp} \sim 4 \times 10^9$ cm/s, and the corresponding kinetic energy of carbon ions $\mathcal{E}_{\rm imp} \sim 100$ MeV.

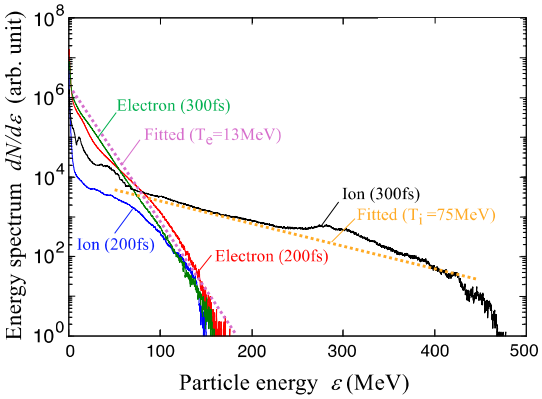

FIG. 4. Energy spectra for ions and electrons, corresponding to the two different times - slightly before ($t = 200$ fs) and slightly after ($t = 300$ fs) the rising of the strong magnetic field at the center. Figure 3 shows the corresponding 2D maps of key physical quantities at the two respective times.

Meanwhile, the ion energy spectrum at $t = 300$ fs in Fig. 4, corresponding to $T_i \approx 75$ MeV (compare the fitted curve) for the energy range 100 MeV$\lesssim \varepsilon \lesssim$ 400 MeV, makes a striking contrast to the ion spectrum at $t = 200$ fs. This strong heating of ions and the generation of strong magnetic field at the center coherently occur. In other words, when the imploding ions are passing by the closest points to the center, the local density quickly increases to reach the same order of the solid density, and at the same time strong currents induced by both the ions and electrons generate the ultrahigh magnetic fields. The magnetic fields thus generated then trap the ions, which convert a substantial amount of their own imploding kinetic energy into thermal energy via ion-ion collisions. As a result, the ions remain tightly trapped by the self-generated magnetic field on the order of sub-megatesla, and are confined in this region for a duration exceeding a few picoseconds, which is substantially longer than the pulse duration of the applied laser (∼100 fs).

The generation and saturation of the axial magnetic field can be interpreted as a feedback loop: ion and electron flow induced by the blades drive azimuthal currents, which generate axial magnetic fields, compressing the plasma further. This positive feedback continues until the system reaches a saturated state.

As the self-generated axial magnetic field increases, the Larmor radii of both electrons and ions shrink, confining their transverse motion more tightly around the axis. This magnetic confinement effectively compresses the plasma into a narrower region, thereby increasing the local current density and enhancing the magnetic field.

III. CONCLUSION

We have proposed and validated a novel target design—the bladed microtube (BMI) scheme—for the generation of gigagauss-level magnetic fields using laser-plasma interaction. The introduction of periodic blade structures induces a geometric asymmetry that breaks the symmetry of electron and ion flows, resulting in the formation of a strong loop current and the subsequent generation of an intense axial magnetic field.

Particle-in-cell (PIC) simulations have demonstrated that this geometry-driven mechanism can self-consistently amplify magnetic fields up to 450 kT without requiring any external seed field. An analytic model was developed to interpret the underlying dynamics and predict scaling laws, revealing a feedback loop between magnetic confinement and current enhancement.

This BMI concept opens a new path to compact, laser-driven, strongly magnetized plasmas, with potential applications ranging from inertial confinement fusion and laboratory astrophysics to high-field material science. The present study thus lays a robust theoretical and computational foundation for future experimental implementations.

REFERENCES

[1] G. Gregori, B. Reville, and F. Miniati, Physics Reports **601**, 1 (2015).
[2] V. Prat, S. Mathis, B. Buysschaert, J. Beeck, D. Bowman, C. Aerts, and C. Neiner, Astronomy & Astrophysics **635**, A106 (2020).
[3] K. Li, Z. Liu, Y. L. Yao, Z. Zhao, C. Dong, D. Li, S. Zhu, X. T. He, and B. Qiao, Nuclear Fusion **62**, 076008 (2022).
[4] W. Chen and Z. Wang, Chinese Physics Letters **37**, 125001 (2020).
[5] L. Comisso, G. R. Farrar, and M. Muzio, arXiv:2401.08913 (2024), preprint.
[6] Z.-Q. Huang, B. Reville, J. Kirk, and G. Giacinti, Mon. Not. R. Astron. Soc. **524**, 1731 (2023).
[7] H. Feng, Z. Zhou, Y. Wu, Z.-J. Gao, Y. Liang, N. Huang, L. Yan, H. Deng, Y. Du, R. Li, W. Lu, W. Huang, and C. Tang, Physical Review Applied **15**, 044032 (2021).
[8] M. Murakami, J. J. Honrubia, K. Weichman, A. V. Arefiev, and S. V. Bulanov, Scientific Reports **10**, 16653 (2020).
[9] Y. Gu and M. Murakami, Scientific Reports **11**, 23592 (2021).
[10] A. D. Sakharov, Soviet Physics Uspekhi **9**, 294 (1966).
[11] O. V. Gotchev, J. P. Knauer, P. Y. Chang, D. D. Meyerhofer, and R. Betti, Physical Review Letters **103**, 215004 (2009).
[12] J. P. Knauer, O. V. Gotchev, P. Y. Chang, D. D. Meyerhofer, and R. Betti, in *51st Annual Meeting of the APS Division of Plasma Physics* (Atlanta, GA, USA, 2009) abstract available at `https://meetings.aps.org/Meeting/DPP09/Session/GP8.43`.
[13] T. D. Arber, K. Bennett, C. S. Brady, A. Lawrence-Douglas, M. G. Ramsay, N. J. Sircombe, P. Gillies, R. G. Evans, H. Schmitz, A. R. Bell, and C. P. Ridgers, Plasma Physics and Controlled Fusion **57**, 113001 (2015).
[14] S. C. Wilks, W. L. Kruer, M. Tabak, and A. B. Langdon, Physical Review Letters **69**, 1383 (1992).